The universal equilibrium spectra of turbulent velocity and scalar fields

By C. H. GIBSON AND W. H. SCHWARZ
Department of Chemical Engineering, Stanford University, Stanford, California

(Received 30 July 1962 and in revised form 17 January 1963)

Kolmogoroff's (1941) theory of local isotropy and universal similarity predicts that all turbulent velocity spectra are reducible to a single universal curve for the highest wave-numbers and that under certain conditions dimensional analysis may be used to predict spectral shapes. Identical arguments predict that the fine structure of conserved dynamically passive scalar fields mixed by turbulence will also be universally similar.

A single-electrode conductivity probe in a bridge circuit was used to measure the spectra and decay of a random homogeneous field of concentration and temperature behind a grid, and a Lintronic constant-temperature hot-film anemometer was used to measure the decay of velocity field. These experimental measurements of absolute turbulent velocity, temperature, and concentration spectra in salt water are here compared with the general predictions of universal similarity and local isotropy theories, as well as a prediction by Batchelor (1959) of the exact large wave-number spectral form for scalar mixing at high Schmidt number ($\nu \gg D$). The spectral shapes are found to have the predicted similarity forms, and the data are consistent with Batchelor's predicted spectrum of the scalar field.

1. Introduction

It was proposed by Kolmogoroff (1941) that, at sufficiently high Reynolds number, statistical parameters describing the fine structure of fluids in turbulent flow, such as the velocity spectrum at high wave-number, should become universal when the co-ordinates are transformed with length and time scales based on two parameters of the flow field: ϵ, the rate of viscous dissipation of turbulent kinetic energy; and ν, the kinematic viscosity of the fluid. According to the theory, small eddies are formed by the interaction of large eddies generated in the creation of the turbulence, but become statistically independent of the directional details of the large eddies, or 'locally isotropic', as their sizes decrease.

Kolmogoroff's first similarity hypothesis predicts universal fine structure after co-ordinate transformation to length scale $\eta = (\nu^3/\epsilon)^{\frac{1}{4}}$ and time $\sigma = (\nu/\epsilon)^{\frac{1}{2}}$. His second similarity hypothesis is concerned with an intermediate 'inertial' range of eddies with structure independent of kinematic viscosity as well as direction. Fourier energy-spectrum functions should be proportional to wave-number to the $-\frac{5}{3}$ power as a consequence of Kolmogoroff's second hypothesis. These ideas

are well described by Batchelor (1953) who treats the universal equilibrium of velocity spectrum functions whereas Kolmogoroff's discussion was in terms of product moments of velocity differences, or 'structure functions' of the velocity field. Batchelor (1953) demonstrated the equivalence of universal-similarity hypotheses applied to either the structure function or the spectrum function.

Equivalent notions may be applied to the fine structure of scalar fields (such as concentration or temperature) mixed by a turbulent velocity field. In this case, two more parameters are required besides ϵ and ν: χ, the rate of dissipation of scalar variance by diffusion, and D, the molecular diffusivity of the scalar fluid property (with units of length^2/time). Corrsin (1951) and Obukoff (1949) independently predicted a scalar inertial subrange, equivalent to the velocity inertial subrange of Kolmogoroff's second hypothesis, where the scalar variance spectrum is proportional to the wave-number to the $-\frac{5}{3}$ power. For weakly diffusive scalars ($D/\nu \ll 1$), Batchelor (1959) succeeded in extending the consequences of local isotropy and universal similarity to obtain an exact equation for the equilibrium scalar spectrum at very high wave-numbers by integrating the linear scalar diffusion equation for a typical small scalar Fourier element in pure strain. Corrsin (1961) applied local isotropy and Batchelor's procedure ($D/\nu \ll 1$) to obtain the spectral form for the reactant concentration in turbulent mixing with a first-order reaction.

The validity of Kolmogoroff's hypotheses has been challenged by Kraichnan (1959), who employed a 'direct-interaction approximation' to predict an inertial subrange for the velocity spectrum with slope $-\frac{3}{2}$ rather than $-\frac{5}{3}$ (on a log-log plot).

The purpose of this paper is to present the results of some absolute measurements of velocity and scalar spectra for comparison with the general predictions of local-isotropy and universal-similarity theory, as well as with Batchelor's predicted spectrum of a scalar field with Schmidt number $\gg 1$. In addition to the spectral measurements, the law of decay of the scalar variance has been obtained for the range of variables encountered in the present work; namely, grid turbulence in the initial period at grid Reynolds numbers from 10,000 to 70,000, concentration and temperature mixing in dilute salt water for two grid mesh sizes. For a complete discussion, see Gibson (1962).

2. Experiment

A schematic diagram of the experimental equipment is shown in figure 1. Dilute salt water is circulated in a closed-loop water tunnel through the test section where measurements of the velocity and scalar fields are made with suitable detection equipment. Velocity fluctuations are damped by a set of screens and a nine-to-one area contraction before the grid. A biplane grid of perforated tubes which generates the velocity field also generates the scalar fields by the injection of concentrated or heated salt solution through small holes drilled in the tubes. Make-up water was added during concentration injection to maintain a constant background concentration.

Before a run, the tunnel was filled with demineralized water from a 1000 gallon reservoir located next to the water tunnel. During the run, this tank served as

the source of make-up water which was introduced into the system upstream of the main pump. Since the temperatures of the liquid in the tunnel and the make-up water were very nearly the same, and since a degree of mixing was achieved by the pump and subsequent screens in the calming section, it was found that during a concentration-mixing run, the temperature fluctuations seen by the probe were insignificant compared to the signal produced by the salinity fluctuations. An experiment was performed to view the fluctuations or 'noise' seen by the probe when no salt water was injected through the grid but with make-up water flowing into the system. The output voltage for that case was well below that of the main signal. No make-up water was added during the temperature mixing runs.

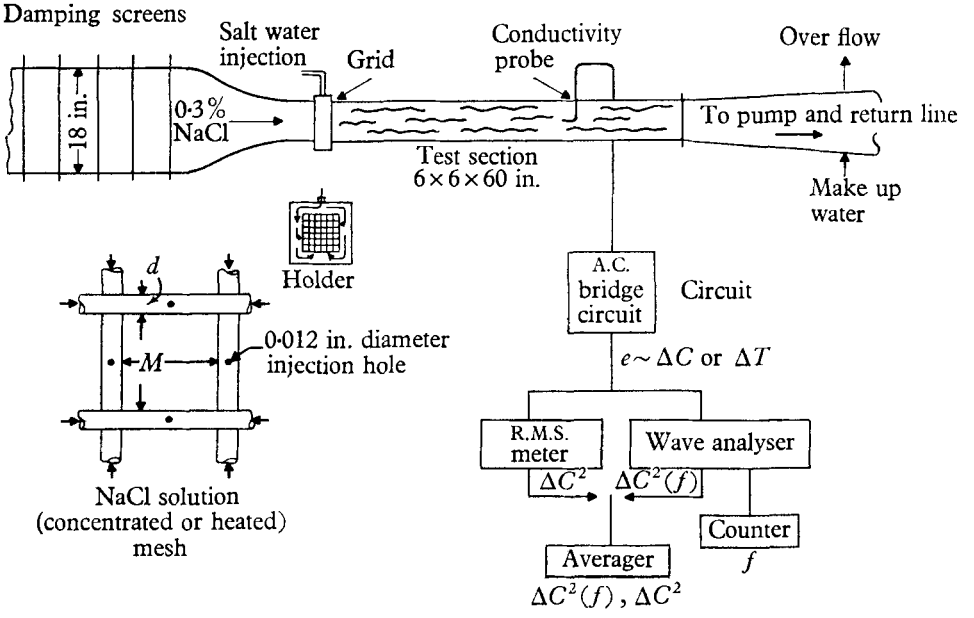

FIGURE 1. Schematic diagram of experimental equipment.

Velocity fluctuations were detected with a Lintronic constant-temperature hot-film anemometer (Ling 1955) in place of the A.C. bridge shown in figure 1, and the mean square and mean power spectrum were measured directly with the analogue equipment shown. The probe was in the form of a 30° wedge on each side of which a platinum film about $1 \times 0{\cdot}2$ mm, 2×10^{-6} cm thick and with a resistance of about 20 Ω. A Hewlett–Packard 302 A heterodyne wave analyser with a bandwidth (area under power transfer function) of 6·10 c/s, was used to measure power spectra. The means of fluctuating output signals of the wave analyser and the Ballantine 320 R.M.S. meter were evaluated using an analogue averaging circuit with time constant adjustable from 2 sec to 30 min.

Since conductivity of salt water is a function of both concentration and temperature, both temperature and concentration fluctuations could be detected with conductivity probes such as that shown in figure 2(*a*), plate 1. The shielded lead from the A.C. bridge is connected to a 0·010 in. platinum lead running through

the $\frac{1}{4}$ in. glass tube to the $10\,\mu$ electrode wire in the cast epoxy tip shown in figure 2(*b*), plate 2. Before use, this tip must be sharpened and platinized under a microscope since it was somewhat rounded by polishing. Its operation depends on the fact that the resistance between the electrode and the grounded tunnel wall is determined primarily by the resistivity of the solution at the electrode surface. Fluctuations in the resistivity of the solution near the probe tip generate a carrier-suppressed amplitude-modulated signal across the balanced A.C. bridge circuit which is suitably demodulated to give a proportional electrical signal. The mixing signal is analysed for mean square and power spectrum in the same manner as the velocity signal. A complete description of the development of the measurement technique is given by Gibson & Schwarz (1963).

The A.C. bridge was a Tektronix Type Q Transducer and Strain Gage plug-in unit in a Model 531 A oscilloscope. The carrier frequency of the bridge was 25 kc/s, limiting the signal frequencies to less than 6 kc/s. The noise level over the band width (2 c/s–6 kc/s) of the circuit was equivalent to an R.M.S. concentration fluctuation c'/C of 0·003 % or an R.M.S. temperature fluctuation t' of 0·001 °C.

One way of testing the predictions of Kolmogoroff's similarity hypotheses for the velocity field is to measure absolute one-dimensional power spectra $\phi(k_1)$ under conditions of known dissipation rate ϵ, where

$$\epsilon = -\tfrac{1}{2}\overline{dq^2}/dt = -\tfrac{3}{2}\overline{du^2}/dt$$

in decaying homogeneous isotropic turbulence, and

$$\int_0^\infty \phi(k_1)\,dk_1 = \overline{u^2}.$$

According to the first similarity hypothesis, high wave-number spectra plotted as $\phi(k_1)\,k_s^3\nu/\epsilon$ versus k_1/k_s should be universal. The symbol $k_s = 1/\eta = (\epsilon/\nu^3)^{\frac{1}{4}}$ is called the Kolmogoroff wave-number and is often used to represent the location of the viscous region of the spectrum. Present indications are that the viscous cut-off occurs at approximately $k = 0{\cdot}1k_s$. Kolmogoroff's second similarity hypothesis predicts an inertial subrange of the normalized spectrum with slope $-\frac{5}{3}$ on a log-log plot for turbulence at sufficiently high Reynolds numbers. It is often stated that laboratory turbulence cannot be produced at high enough Reynolds number to exhibit any such subrange.

Local-isotropy and Kolmogoroff-like similarity hypotheses applied to the spectra of weakly diffusive scalar fluid properties may be tested by measuring the one-dimensional scalar spectrum $\phi_\theta(k_1)$ $\left(\text{where } \int_0^\infty \phi_\theta(k_1)\,dk_1 = \overline{\theta^2}\right)$ under conditions of known dissipation rates for both the turbulent kinetic energy and scalar variance. Arguments similar to the first similarity hypothesis predict that high wave-number spectra of weakly diffusive scalars become universal when plotted as

$$\frac{\phi_\theta(k_1)\,k_s^3\,\nu}{\chi(D/\nu)^{\frac{1}{2}}} \quad \text{versus} \quad \frac{k_1}{k_s}\left(\frac{D}{\nu}\right)^{\frac{1}{2}},$$

where D is the diffusivity of the scalar fluid property. When D is much smaller than ν, it may be shown (Batchelor 1959) that a universal viscous-convective subrange should exist where

$$\frac{\phi_\theta(k_1)\, k_s^3 \nu}{\chi(D/\nu)^{\frac{1}{2}}} \quad \text{is proportional to} \quad \left[\frac{k_1}{k_s}\left(\frac{D}{\nu}\right)^{\frac{1}{2}}\right]^{-1}.$$

In addition, arguments equivalent to the second similarity hypothesis predict (Corrsin 1951; Obukhoff 1949) a scalar inertial subrange at high Reynolds numbers where the spectrum $\phi_\theta(k_1)\, k_s^3 \nu/\chi$ versus k_1/k_s should be universal with $\phi_\theta(k_1)$ proportional to $k_1^{-\frac{5}{3}}$. Thus, local isotropy, similarity hypotheses, and Batchelor's scalar spectrum may be tested by measuring $\phi(k_1)$ and $\phi_\theta(k_1)$ under known conditions of ϵ, χ, ν and D.

3. Velocity-field results

A co-ordinate transformation to length and time scales η and σ should convert turbulent spectra $\phi(k_1)$ to a universal function $\phi_e(k_1')$ for high wave-numbers according to Kolmogoroff's first hypothesis. That is

$$\phi(k_1)\,\sigma^2/\eta^3 = \phi'(k_1') = \phi_e(k_1'), \tag{1}$$

where $\eta = (\nu^3/\epsilon)^{\frac{1}{4}}$, $\sigma = (\nu/\epsilon)^{\frac{1}{2}}$, and the primed quantities are in the prime co-ordinate system $x_i' = x/\eta$, $t' = t/\sigma$.

Using the hot-film anemometer, three measurements were made of $\phi(k_1)$ behind the 1·59 cm mesh grid corresponding to mesh distances of 80, 40 and 20, grid Reynolds numbers of about 20, 30 and 40 thousand, and Kolmogoroff wave numbers of 40, 90 and 170 cm^{-1}, respectively. Dissipation rates were computed by differentiating the linear decay law determined by Batchelor & Townsend (1948) behind geometrically similar grids (mesh-to-rod-diameter ratio 16 : 3) using hot-wire anemometers, viz.

$$U^2/\overline{u^2} = 135[x/M - 10], \tag{2}$$

where U is the mean velocity, u is the downstream fluctuating component of the velocity, x is the distance from the grid, and M is the mesh length or spacing of the round grid bars (see figure 1). Using $x = Ut$, (2) may be differentiated to give the rate of decay of turbulent kinetic energy as a function of distance behind the grid

$$\epsilon = -\frac{3}{2}\frac{d}{dt}[\overline{u^2}(t)] = \frac{1}{90}\frac{U^3}{M}\left(\frac{x}{M} - 10\right)^{-2}. \tag{3}$$

From (3) the Kolmogoroff scales η and σ may be found by the following relations

$$\eta = 3{\cdot}08M(UM/\nu)^{-\frac{3}{4}}(x/M - 10)^{-\frac{1}{2}}, \quad \sigma = \eta^2/\nu, \tag{4}$$

to permit scaling of the spectra to universal form by equation (1).

The normalized velocity spectra taken in the water tunnel are plotted in figure 3, along with several normalized spectra measured behind geometrically similar grids in wind tunnels by Stewart & Townsend (1951) and a spectrum published recently by Grant, Stewart & Moilliet (1962) measured in a tidal channel. There have been no corrections for finite length of probe applied to the

spectra measurements. An analysis similar to that of Uberoi & Kovasnay (1953) for a finite hot-wire does not appear to be readily extended to the geometry of the hot-film. However, from the uncorrected data in figure 3, the correction for

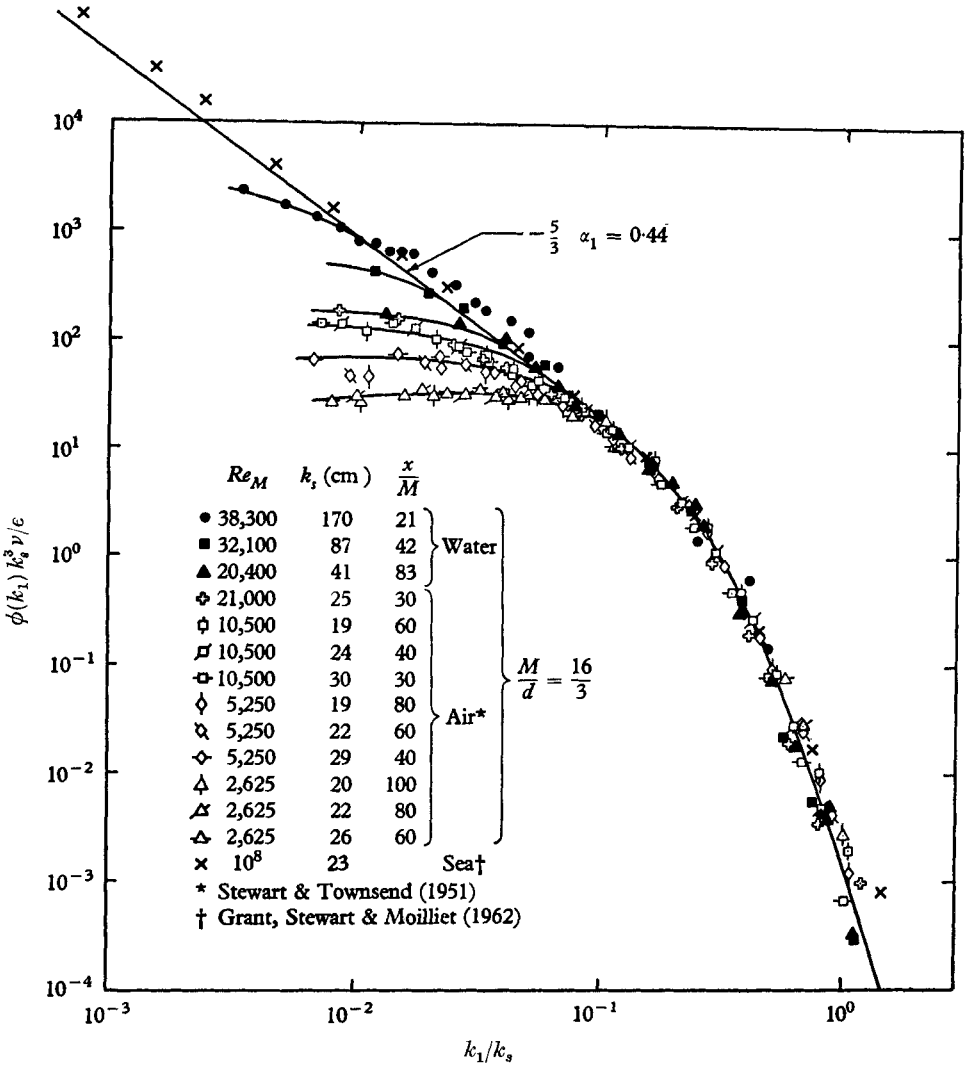

FIGURE 3. Normalized velocity spectra.

finite length of the hot-film should be very similar to that for the hot-wire since the data appear to be similar. The Stewart & Townsend spectra were computed from published measurements of the spectra of the first and second derivatives of the velocity fluctuations. The dissipation rates were calculated by Stewart & Townsend using (3). The Grant, Stewart & Moilliet (GSM) spectrum was normalized using their published values of ϵ and ν. It was obtained from their longest continuous tape recording (15 min) of the velocity signal (09.05, 3. x. 1959).

The agreement of the high wave-number ranges of all the spectra is quite good, providing evidence for the validity of Kolmogoroff's first similarity hypothesis.

The last two points of the ocean spectrum are somewhat higher than the universal spectrum indicated by the grid-turbulence data in water and air, but this may be attributed to noise by inspecting other ocean spectra at higher wave-numbers where the influence of noise is apparent (GSM, p. 256, figure 12).

The choice of the parameter ϵ to characterize the dependence of the fine structure of the velocity field on the large structure was predicated on the notion that the turbulent kinetic energy generated at low, anisotropic wave-numbers is transferred undiminished to the high, isotropic wave-numbers where it is degraded to heat by the viscous forces. Clearly, this representation can be strictly correct only under conditions of high Reynolds number. The basic notion that the fine structure of turbulence will be independent of the details of the large structure should be valid even at low Reynolds numbers, but to normalize such a spectrum to the universal curve shown in figure 3, the proper dissipation rate would be the value corresponding to an infinite Reynolds-number flow system with the same high wave-number spectrum as the actual flow, rather than the true dissipation rate. Hence, since true dissipation rates were used to normalize the low Reynolds-number flows of figure 3 rather than rates computed, say, from the spectrum obtained by extrapolating the actual spectrum according to the GSM curve, the good agreement of the high wave-numbers curves for high and low Reynolds-number flows in figure 3 might seem contradictory to local-isotropy theory. The contradiction is resolved, however, by examining the dissipation spectrum of the universal curve (Stewart & Townsend, p. 370, figure 5) and the fact that the normalization factors only depend on ϵ to the one-fourth power. Hence, as long as the 'energy-containing eddies' have wave number less than about $0{\cdot}2k_s$, the 'low Reynolds number' correction to the normalized spectrum will be negligible.

At lower wave numbers, the low Reynolds-number spectra begin to depart from the universal, infinite Reynolds-number curve. At a given grid Reynolds number, the normalized spectra for different x/M values apparently coincide, indicating self-preservation. The water and air grid spectra at the same Reynolds number agree at high and low wave-number but disagree somewhat near the intersection with the universal curve. The difference might be due to the difference in wave analyser bandwidths, since the ratio of bandwidth to intersection frequency for the water data was one-sixth, compared to one-half for the air data.

As the Reynolds number of the turbulence increases, the spectra exhibit increasing universal portions, departing asymptotically from the same inertial subrange curve of slope $-\frac{5}{3}$ predicted by Kolmogoroff's second hypothesis. The data of Grant, Stewart & Moilliet, taken at a Reynolds number based on the depth of their tidal channel of 10^8, exhibit several decades of the spectrum with this slope. The regularity of the data is quite adequate to distinguish between slopes of $-\frac{5}{3}$ and $-\frac{3}{2}$, supporting Kolmogoroff's theory rather than Kraichnan's. The fact that a portion of the water-tunnel spectrum at grid Reynolds number 38,300 is somewhat higher than the rest of the data is attributed to a temporary change in the hot-film sensitivity, since none of the other spectra exhibit the peculiar humped shape which has to be drawn if this portion of the spectrum is believed. With this interpretation, the asymptotical $-\frac{5}{3}$ slope line shown in

figure 3 was drawn for the grid-turbulence spectra corresponding to a universal one-dimensional Kolmogoroff constant $\alpha_1 = 0{\cdot}44 \pm 0{\cdot}02$ for the grid-turbulence data, where α_1 is defined by

$$\phi_e(k_1') = \alpha_1 k_1'^{-\frac{5}{3}} \tag{5}$$

in the inertial subrange. This may be compared to a value of about 0·5 for the ocean spectrum shown in figure 3 and average values of $0{\cdot}47 \pm 0{\cdot}02$ and 0·424 published by Grant, Stewart & Moilliet in different reports of their measurements (1962, 1960, respectively).† The corresponding three-dimensional Kolmogoroff spectrum constant α_3, defined by

$$E'(k') = E(k)\,\sigma^3/\eta^2 = \alpha_3(k\eta)^{-\frac{5}{3}} \tag{6}$$

may be shown to be $55/18\alpha_1$; thus $\alpha_3 = 1{\cdot}34 \pm 0{\cdot}06$.

The constant values approached by the one-dimensional grid spectra as k_1 approaches zero may be shown to be

$$\phi(0) = 2\pi^{-1}\overline{u^2}\Lambda, \tag{7}$$

where Λ is the longitudinal integral scale $\int_0^\infty f(r)\,dr$; and

$$f(r) = \overline{u_r(\mathbf{x})\,u_r(\mathbf{x}+\mathbf{r})}/\overline{u_r^2}.$$

If we define the wave-number k_0 corresponding to the intersection of

$$\phi(k_1) = 2\pi^{-1}\overline{u^2}\Lambda$$

with the universal inertial subrange line, then we can show that

$$k_0 = k_s(0{\cdot}44\pi/2R_\eta R_\Lambda)^{\frac{3}{5}}, \tag{8}$$

where $R_\eta = u'\eta/\nu$ and $R_\Lambda = u'\Lambda/\nu$. Since the beginning of the viscous subrange occurs at $k_1/k_s = 0{\cdot}1$, an inertial subrange can exist in a particular flow only if it is possible to find (normalized) wave numbers k_1' that lie between k_0' and 0·1, that is, only if $k_0' < 0{\cdot}1$. Thus a criterion for the existence of an inertial subrange is

$$R_\lambda \gg 567, \tag{9}$$

since $R_\eta = 0{\cdot}43R_\lambda^{\frac{1}{2}}$, $R_\lambda = u'\lambda/\nu$ and R_λ and R_Λ may be approximated by (Batchelor & Townsend 1948) $R_\Lambda \doteq 0{\cdot}1R_\lambda^2$.

4. Universal equilibrium hypotheses for the scalar field

The notions of local isotropy and Kolmogoroff-like similarity hypotheses for the structure of weakly diffusive scalar fields mixed by turbulent velocity fields may be supplemented by the arguments furnished by Batchelor (1959). Batchelor recognized that when $D/\nu \ll 1$, fluctuations of a scalar fluid property Θ may

† *Editors' note.* As remarked in the text, the value of the Kolmogoroff constant given by Grant, Stewart & Moilliet in their 1962 paper (*J. Fluid Mech.* **12**, 241) differs from that given in their 1960 unpublished report (Pac. Nav. Lab., Report 60–8). These authors have informed the editors that the results given in the 1960 report were calculated with an incorrect value of the kinematic viscosity, and that this report should be regarded as superseded by the paper published in 1962.

exist at a much finer scale than fluctuations of velocity. Hence, the smallest scalar fluctuations will be convected by pure strain, since it is very unlikely that they will find themselves in a region of the fluid where the velocity fluctuations in space are as frequent as the fluctuations of the scalar. Through the analysis of the history of a single high wave-number Fourier element of the scalar field in pure strain, Batchelor showed that the most important quantity in the convection is the value of the least principal rate of strain γ of the strain tensor e_{ij}, where

$$e_{ij} = \frac{1}{2}\left(\frac{\partial u_i}{\partial x_j} + \frac{\partial u_j}{\partial x_i}\right) \quad (i, j = 1, 2, 3).$$

When the co-ordinates are transformed to the 'principal axes'

$$e_{ij} = \begin{bmatrix} \alpha & 0 & 0 \\ 0 & \beta & 0 \\ 0 & 0 & \gamma \end{bmatrix},$$

where the x_3-axis has been chosen to coincide with the direction of the principal axis of the least strain γ, which is necessarily negative by continuity since $e_{ii} = 0 = \alpha + \beta + \gamma$ for an incompressible fluid.

By assuming that the scalar field at high wave-number was under the influence of the same least principal rate of strain, Batchelor was able to predict the following equation for the equilibrium three-dimensional scalar spectrum function $\Gamma(k)$

$$\Gamma(k) = -\frac{\chi}{\gamma}\frac{1}{k}\exp\left(\frac{D}{\gamma}k^2\right), \tag{10}$$

where k is the wave-number magnitude, $\int_0^\infty \Gamma(k)\,dk = \overline{\theta^2}$, $\overline{\theta}(\mathbf{x}, t) = 0$, and γ denotes the effective average least principal rate of strain of the velocity field. Batchelor further suggested that the effective value of γ would be $-\frac{1}{2}(\epsilon/\nu)^{\frac{1}{2}}$, giving a definite expression for the high wave-number spectrum

$$\Gamma(k) = \frac{2\chi}{k(\epsilon/\nu)^{\frac{1}{2}}}\exp\left[\frac{-2Dk^2}{(\epsilon/\nu)^{\frac{1}{2}}}\right], \tag{11}$$

which for future reference may be written

$$\Gamma'(\omega) = \Gamma(k)\,k_s^3\,\nu/\chi(D/\nu)^{\frac{1}{2}} = (2/\omega)\exp(-2\omega^2), \tag{12}$$

where $\omega = (D/\nu)^{\frac{1}{2}}\,k/k_s$.

The mixing problem may be considered in terms of Kolmogoroff-like similarity hypotheses. A dynamically passive, conserved, scalar fluctuation field $\theta(\mathbf{x}, t)$, such as concentration or temperature, generated at a large scale by some external agency, is mixed by the turbulent velocity field $\mathbf{u}(\mathbf{x}, t)$ according to the equation

$$\frac{\partial\theta}{\partial t} + u_i\frac{\partial\theta}{\partial x_i} = D\frac{\partial^2\theta}{\partial x_j\,\partial x_j}, \tag{13}$$

where $\overline{u}_i = \overline{\theta} = \partial u_i/\partial x_i = 0$, and $D \ll \nu$.

The similarity hypothesis for fluctuations of size intermediate between the viscous scale of the velocity field and the diffusive scale of the scalar field should be:

Scalar fluctuations smaller than the viscous scale of the turbulent velocity field should approach a unique statistical equilibrium determined by the parameters χ, γ and D.

By hypothesis, a co-ordinate transformation to length, scalar and time scales formed from the parameters χ, γ and D should collapse all scalar spectra at high wave-numbers to a universal form: possibly that predicted by Batchelor with equation (12). The only possible combinations of the parameters are the scales

$$\left.\begin{array}{ll} \text{length} & l = (D/\gamma)^{\frac{1}{2}}, \\ \text{time} & \tau = \gamma^{-1} l, \\ \text{scalar} & \Sigma = (\chi/\gamma)^{\frac{1}{2}}. \end{array}\right\} \tag{14}$$

Now, performing the co-ordinate transformation

$$\theta' = \theta/\Sigma, \quad t' = t/\tau, \quad L' = L/l, \tag{15}$$

we obtain from the one-dimensional scalar spectrum $\phi_\theta(k_1, t)$, the universal spectrum $\phi_{\theta e}(k_1')$ by the similarity hypothesis

$$\phi_\theta(k_1', t') = \phi_\theta(k_1, t)/\Sigma^2 l = \phi_{\theta e}(k_1'), \tag{16}$$

where $k_1' = k_1 l$.

Assuming that the rate-of-strain parameter γ depends only on ϵ and ν, we may use for γ the only combination of these quantities with the proper units; that is, $\gamma \cong (\epsilon/\nu)^{\frac{1}{2}}$. Equation (16) then becomes

$$\frac{\phi_\theta(k_1, t)\, k_s^3 \nu}{\chi (D/\nu)^{\frac{1}{2}}} = \phi_{\theta e}\left\{\frac{k_1}{k_s}\left(\frac{D}{\nu}\right)^{\frac{1}{2}}\right\} \tag{17}$$

which may be compared to (12).

If the diffusion and viscous wave-numbers are widely separated, there should exist a range of wave-numbers which are independent of the diffusivity D and depend only on γ and χ. As pointed out by Batchelor (1959), this requires that

$$\frac{\phi_\theta(k_1, t)\, k_s^3 \nu}{\chi (D/\nu)^{\frac{1}{2}}} = \beta_2 \left\{\frac{k_1}{k_s}\left(\frac{D}{\nu}\right)^{\frac{1}{2}}\right\}^{-1}; \tag{18}$$

the particular form (10) reduces to (18) when $k \ll (\gamma/D)^{\frac{1}{2}}$.

Corrsin (1951) and Obukhoff (1949) independently predicted the existence of a scalar inertial subrange for mixing systems with very high Reynolds number, where the scalar spectrum is independent of both D and ν and depends only on ϵ and χ.

The indicated spectrum

$$\phi_\theta(k_1, t)\, k_s^3 \nu/\chi = \beta_1 (k_1/k_s)^{-\frac{5}{3}} \tag{19}$$

is valid for all scalars, even those with $D > \nu$.

The results of the similarity hypotheses given by equations (19), (18) and (17) are summarized graphically in figure 4, where the normalized universal equilibrium spectra are shown plotted as $\phi_\theta k_s^3 \nu/\chi$ versus k_1/k_s in figure 4(*a*) to

illustrate the universal scalar inertial and viscous-convective subranges. Figure 4(*b*) is a plot of

$$\frac{\phi_\theta k_s^3 \nu}{\chi(D/\nu)^{\frac{1}{2}}} \text{ versus } \frac{k_1}{k_s}\left(\frac{D}{\nu}\right)^{\frac{1}{2}}$$

illustrating the universal viscous-convective and diffusive subranges. The spectra shown are for three scalars with different diffusivities, all small compared to the kinematic viscosity of the fluid, mixed at large Peclet number Lu'/D, where L is the length scale of the largest scalar fluctuation, and with the assumption that the rate-of-strain parameter necessary to produce similarity is $(\epsilon/\nu)^{\frac{1}{2}}$.

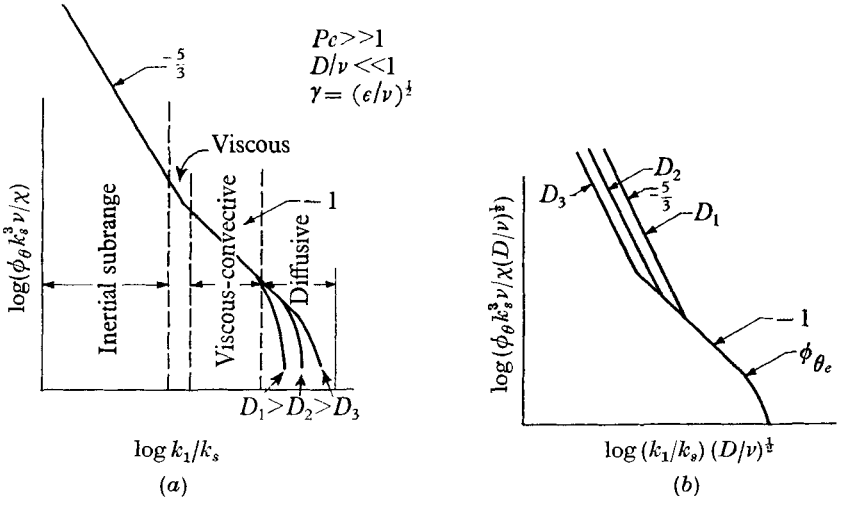

FIGURE 4. Universal scalar spectra at high Schmidt number: (*a*) inertial and viscous-convective subranges; (*b*) viscous-convective and diffusive subranges.

5. Decay of the scalar field

From figure 4, it is apparent that to normalize properly measured spectra of scalar mixing, it is necessary to know the dissipation rate of θ-variance. In general, χ is $-2D\overline{\theta(\partial^2\theta/\partial x_i \partial x_i)}$; however, for a decaying system this becomes $-d\overline{\theta^2}/dt$. Hence, χ may be measured by differentiating the scalar decay law equivalent to the linear decay law for the turbulence, equation (2), found by Batchelor & Townsend (1948).

Figure 5 shows the decay of $\overline{c^2}$ with distance x/M from the grid, where $C(t) = \bar{C} + c(t)$ is the salt concentration at the probe tip. An initial value of $(\overline{c^2})^{\frac{1}{2}}$ is plotted since it may be shown (Gibson 1962, p. 142) that it will be greater than c_0, the known increment in mean concentration across the grid. The conditions of the test are shown on the plot, where $Re_M = UM/\nu$, $\bar{C}$ is the average concentration in the test section, and C_1 is the concentration of the solution injected through the grid. Measurements such as shown in figure 5 and tests of the effects of varying mean velocity, the mesh size, the diffusivity of the scalar (through the use of temperature decay) and the injection rate, indicated the following scalar decay law

$$\overline{\theta^2}/\theta_0^2 = 3{\cdot}10(x/M)^{-\frac{3}{2}} \tag{20}$$

for the range of variable encountered in the present system. In (20), θ_0 is the increment in the mean value $\overline{\Theta}$ of the scalar fluid property $\Theta(t) = \overline{\Theta} + \theta(t)$ of the main stream, caused by the injection of concentrated scalar as it passes through the grid. The apparent origin of the scalar field did not seem to differ significantly from $x = 0$.

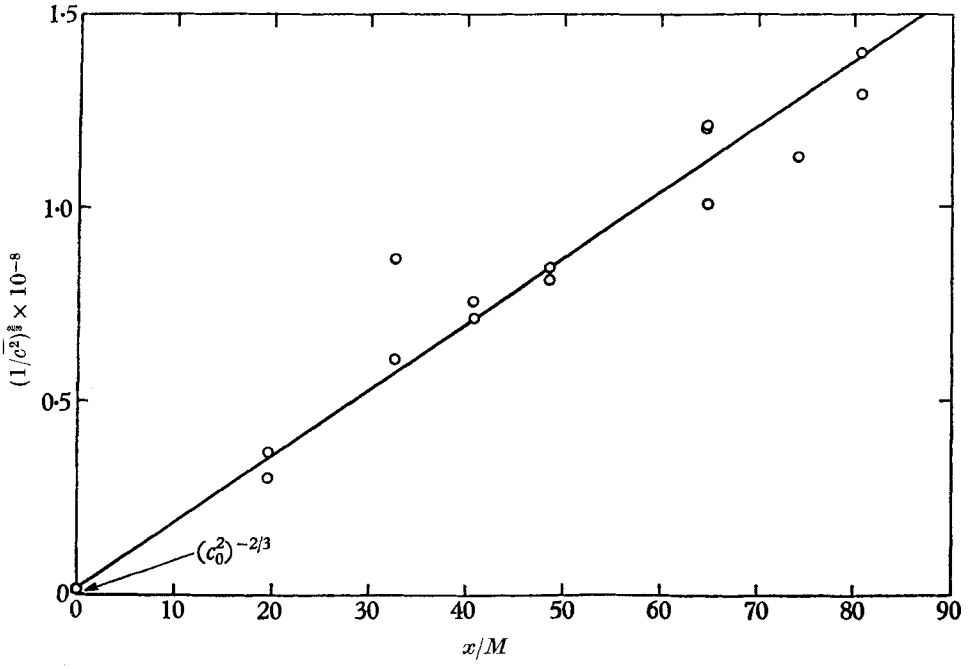

FIGURE 5. Decay of concentration fluctuations behind grid.
$Re_M = 10{,}200$; $\overline{C} = 0{\cdot}26$ %; $C_1 = 5{\cdot}8$ %; $M = 1{\cdot}59$ cm.

Hinze (1959, p. 236) shows that by assuming (1) self-preservation of the correlation coefficient, $f_\theta(\mathbf{r}) = \overline{\theta(\mathbf{x})\theta(\mathbf{x}+\mathbf{r})}/\overline{\theta^2}$, and (2) that the Corrsin parameter, $I_C = \overline{\theta^2} = \int_0^\infty r^2 f_\theta(r)\, dr$, is invariant, the decay of scalar variance in the initial period of the turbulence ($x/M < 200$) is proportional to $t^{-\frac{3}{2}}$, where t is the time of decay. For this reason, the $\overline{c^2}$ versus x/M data of figure 5 were plotted as $(\overline{c^2})^{-\frac{2}{3}}$ versus x/M, and the straight line seems to be compatible with the data.

With (2), and using $x = Ut$, the dissipation rate may be calculated

$$\chi = -\frac{d}{dt}(\overline{\theta^2}) = \frac{3}{2}\frac{U}{x}\overline{\theta^2} = \chi_D, \tag{21}$$

where the subscript of χ_D indicates that χ is computed from the decay law. The dissipation rate may also be computed by integrating the 'dissipation spectrum' $k_1^2\phi_\theta(k_1)$ for a given measurement of the scalar spectrum (Hinze 1959, p. 227)

$$\chi = 6D\overline{\theta^2}\int_0^\infty k_1^2 \frac{\phi_\theta(k_1)}{\overline{\theta^2}}\, dk_1 = \chi_S. \tag{22}$$

The ratio of these two expressions for the dissipation is

$$\frac{\chi_S}{\chi_D} = \frac{4Dx}{U}\int_0^\infty k_1^2 \frac{\phi_\theta(k_1)}{\overline{\theta^2}}\,dk_1. \tag{23}$$

Since the integral of the dissipation spectrum is very sensitive to the spectral values at high wave-numbers, equation (23) provides a powerful check on the accuracy of the high wave-number portion of the measured spectrum, where errors due to inadequate spatial resolution of the conductivity probes might be expected.

6. Results

Table 1 shows the operating conditions for six concentration-mixing runs and one temperature-mixing run during which the spectra shown in figure 6 were measured. The basic data measured for these plots were $\phi_\theta(k_1)/\overline{\theta^2}$ since normal-

Run	Mean velocity U (cm/sec)	Grid mesh M (cm)	Distance from grid x/M	$\overline{C}$ (wt. %)	C_1Q (g/sec)	$\frac{UM}{\nu}$	D_e (μ)	k_s (cm^{-1})
CM 1	64	1·588	70	0·1	0·798	11,700	50	29·5
CM 12	127	2·62	19·5	0·293	0·355	35,000	13·9	102
CM 13	240	2·62	19·5	0·305	0·355	65,550	13·1	165
CM 15	125	2·62	19·5	0·309	0·355	35,300	52·8	97·1
CM 16	153	1·588	64·5	0·328	0·366	26,200	35·5	55·7
CM 17	155	1·588	19·5	0·366	0·366	26,500	38	133·5
TM 2	125	2·62	19·5	0·309	0	35,300	52·8	97·1

TABLE 1. Operating conditions for experimental runs

$\overline{C}$ = background concentration
C_1 = injected concentration
Q = injection rate
D_e = apparent diameter of electrode = $(2\pi \times \text{cell constant})^{-1}$
k_s = Kolmogoroff wave-number

izing each spectral point compensates for variations in either sensitivity or signal level. Normalized spectra were computed using (21) and $k_s = 1/\eta$ computed from (4) as follows

$$\frac{\phi_\theta(k_1)\,k_s^3\nu}{\chi} = \frac{\phi_\theta(k_1)}{\overline{\theta^2}}\frac{2}{3}\frac{x}{U}k_s^3\nu. \tag{24}$$

Also plotted in figure 6 is the universal velocity spectrum of figure 3, $\phi(k_1)\,k_s^3\nu/\epsilon$ versus k_1/k_s for comparison with the scalar spectra.

Batchelor's theoretical prediction of the three-dimensional spectrum function $\Gamma(k)$ may be converted to the one-dimensional spectrum function $\phi_\theta(k_1)$ using the relation (Hinze 1959, equation 3–187)

$$\phi_\theta(k_1) = \int_{k_1}^\infty \frac{\Gamma(k)\,dk}{k} \tag{25}$$

with

$$\gamma = -\frac{1}{q}\left(\frac{\epsilon}{\nu}\right)^{\frac{1}{2}},$$

where q is a constant to be determined. Substitute

$$\frac{\Gamma(k)\, k_s^3 \nu}{\chi (D/\nu)^{\frac{1}{2}}} = \frac{q}{\omega} \exp\left(-q\omega^2\right) \tag{26}$$

into (25), where $\omega = (k/k_s)(D/\nu)^{\frac{1}{2}}$, to obtain the normalized one-dimensional spectrum

$$\frac{\phi_\theta(k_1)\, k_s^3 \nu}{\chi q (D/\nu)^{\frac{1}{2}}} = (4\pi q)^{\frac{1}{2}} \left\{ \frac{\Phi\{\omega_1 (2q)^{\frac{1}{2}}\}}{\omega_1 (2q)^{\frac{1}{2}}} - \int_{\omega_1 \sqrt{(2q)}}^{\infty} \Phi(y)\, dy \right\}, \tag{27}$$

where $\Phi(x)$ is the normal probability density function

$$\Phi(x) = 2\pi^{-1} \exp\left(-\tfrac{1}{2}x^2\right). \tag{28}$$

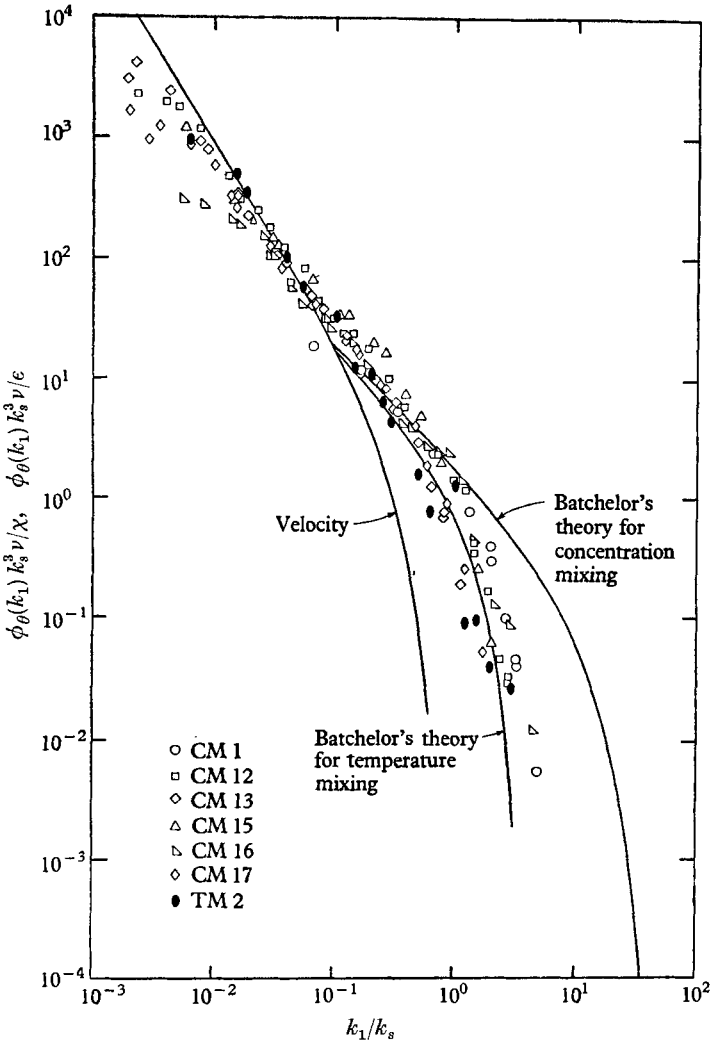

FIGURE 6. Normalized scalar mixing spectra.

From tabulated values of $\Phi(x)$ and $\int_x^\infty \Phi(y)\,dy$, the theoretical spectra for concentration and temperature mixing were computed and are shown plotted in figure 6.

Several interesting features may be noted from figure 6. First, all the scalar-mixing spectra appear to exhibit the universal inertial and viscous-convective

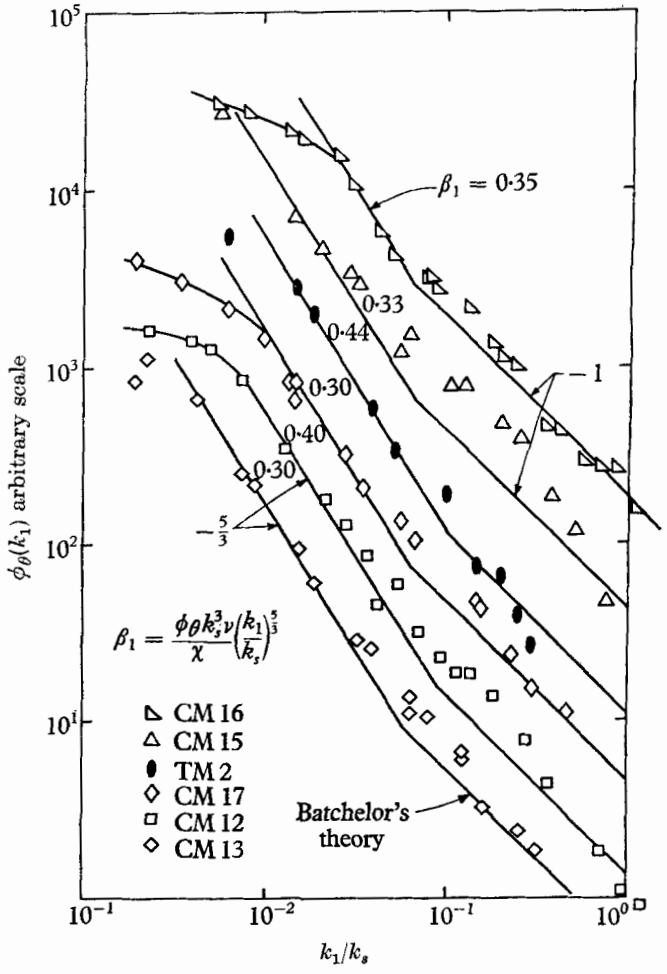

FIGURE 7. Scalar inertial subrange.

subranges predicted using scalar-mixing similarity hypotheses and local isotropy (*figure 4 (b)*). *Sighting along the inertial subrange with the eye close to the paper* will reveal the inflexion in the spectra as the mixing mechanism becomes pure strain after the viscous cut-off of the velocity spectrum. Second, the high wave-number concentration-mixing spectra scatter considerably and all lie below Batchelor's theoretical curve. Computations of the dissipation rates from the various spectra using (23) give χ_S/χ_D ratios ranging between 1 : 20 and 1 : 200, clearly indicating that the measured high wave-number concentration-mixing

spectra are low due to the inability of the conductivity probes to resolve some of the extremely fine concentration fluctuations encountered. For example, for CM 13 the wavelength corresponding to the wave-number above 90% of the dissipation is about 7μ. Nevertheless, the high wave-number concentration-

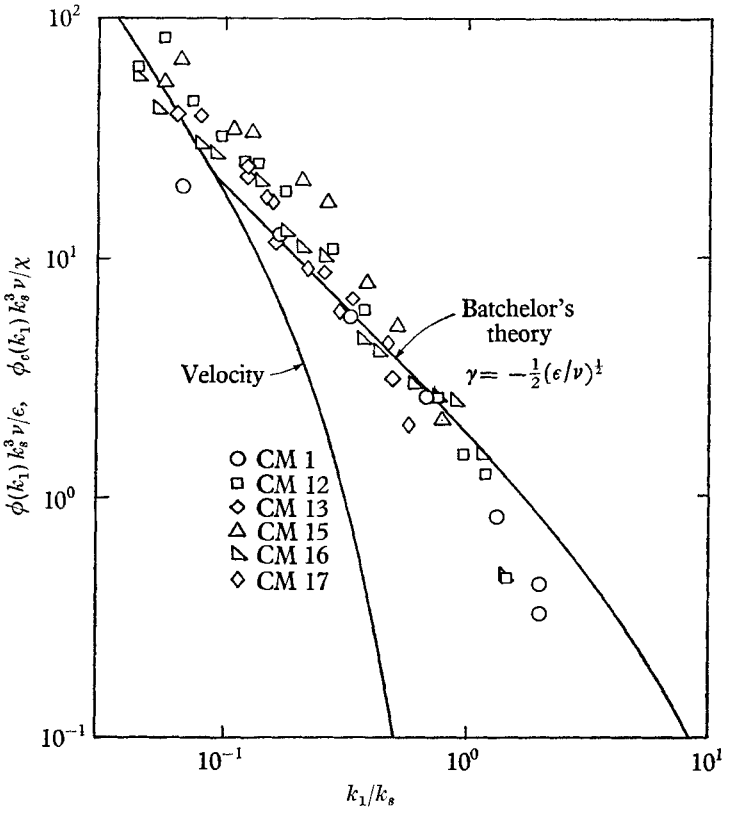

FIGURE 8. Viscous-convective subrange.

mixing spectra are considerably above the velocity and temperature-mixing spectra, and the six absolute spectra shown in figure 6 and eleven other qualitative spectra (Gibson 1962) measured in the course of the experiment are consistent with the predicted viscous-convective slope of -1.

The scalar-mixing spectra which exhibited inertial subranges are shown in figure 7 with arbitrary spectral scales to separate data for the different runs. The best fitting $-\frac{5}{3}$ line was drawn through the inertial subranges of each of the six spectra and the corresponding scalar one-dimensional Kolmogoroff constants $\beta = (\phi_\theta k_s^3 \nu/\chi)\,(k_1/k_s)^{\frac{5}{3}}$ were calculated and are shown on figure 7. The average value was $0{\cdot}35 \pm 0{\cdot}05$ standard deviation. The equivalent three-dimensional constant

$$\beta_3 = \tfrac{5}{3}\beta_1 = \Gamma(k)\,(\epsilon^{\frac{1}{3}}k^{\frac{5}{3}}/\chi),$$

is 0·58. The most extensive inertial subrange was exhibited by run CM 13, taken at $Re_M = 67{,}000$, where the $-\frac{5}{3}$ slope portion of the spectrum extended over a decade of wave-numbers. For reference, the $-\frac{5}{3}$ inertial subrange lines of the

various spectra are extended at high wave-number by Batchelor's spectrum ($\nu/D = 700$).

The viscous-convective regions of the concentration-mixing spectra are shown compared to Batchelor's theory and the universal velocity spectrum in figure 8. All the spectra except CM 15 are in reasonable agreement with Batchelor's

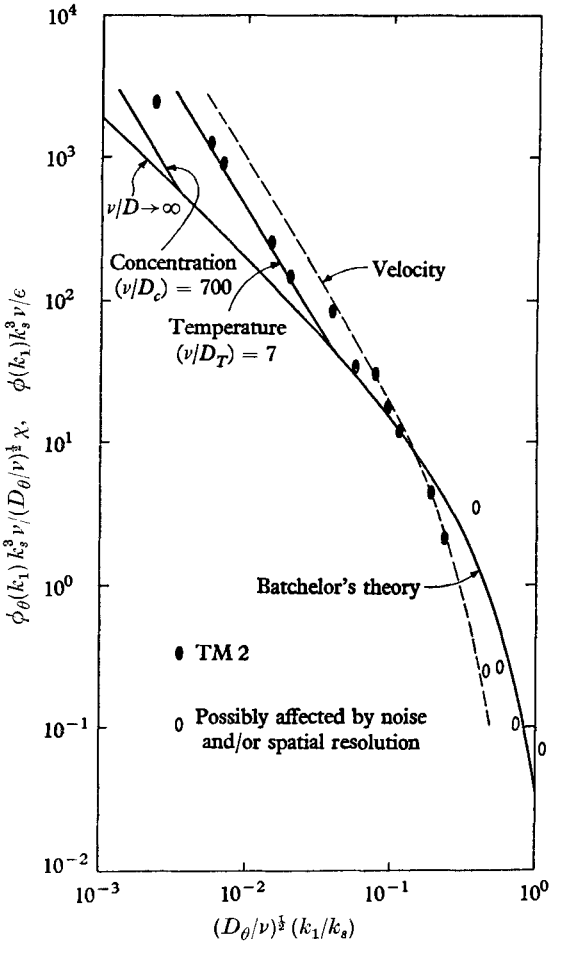

FIGURE 9. Diffusive subrange.

curve. The largest measured values of k_1/k_s which were unaffected by spatial resolution were obtained for runs CM 1 and CM 16 which were also taken at larger values of x/M than the other runs, 70 and 64·5, respectively, so their Kolmogoroff numbers should be more accurate than the others which were taken at x/M values of only about 19·5. The agreement of CM 16 and CM 1 with Batchelor's theory is to within about $\pm 5\,\%$.

Figure 9 is a plot of the normalized scalar mixing ($D/\nu \ll 1$) and velocity spectra plotted in the manner suggested by Kolmogoroff-like similarity hypotheses as discussed previously and illustrated in figure 4 (*b*). Batchelor's spectrum is shown extended to lower wave numbers by a line of slope -1 corresponding

to scalars with nearly zero diffusivity. As expected from figures 4(*b*), the $-\frac{5}{3}$ slope inertial subrange lines for the concentration and temperature spectra intersect the $\nu/D \to \infty$ line at different points due to the difference in their diffusivity ratios ν/D, which were 700 and 7, respectively. The temperature-mixing data of run TM 2 are plotted for comparison with Batchelor's theory. As indicated, some of the high wave-number data may have been affected by noise and/or spatial resolution since the signal level was only $(\overline{\Delta T^2})^{\frac{1}{2}} = 0{\cdot}005\,^{\circ}\mathrm{C}$ (signal-to-noise ratio = 5; $\Delta T_0 = \theta_0 = 0{\cdot}03\,^{\circ}\mathrm{C}$).

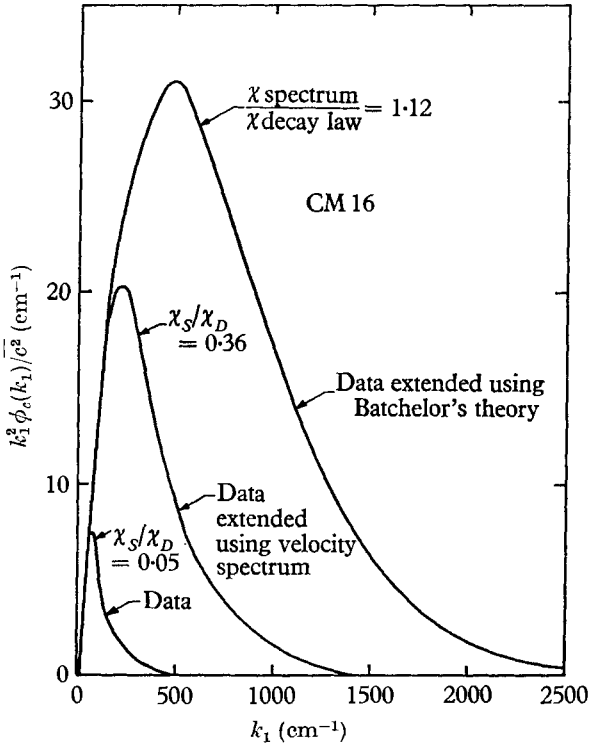

FIGURE 10. Dissipation spectra.

To illustrate the sensitivity of the dissipation ratio χ_S/χ_D to various extrapolations of the high wave-number data, as well as to check the compatibility of the one-dimensional spectrum of equation (27) with the requirement that $\chi_S = \chi_D$, the dissipation spectra for run CM 16 were derived. The actual data were extrapolated to high wave-number using both the velocity and Batchelor's spectrum, the dissipation spectra $\phi_c(k_1)/\overline{c^2}$ were plotted for the data, the velocity extension and Batchelor's extension and the ratios χ_S/χ_D were found to be 0·05, 0·36 and 1·12, respectively (see figure 10). The low value for the raw data demonstrates the failure of the conductivity probes to resolve the smallest fluctuations of concentration. Also, the 0·36 value obtained by extending the scalar spectrum by using the form of the velocity spectrum indicates the incorrectness of this approach. Computations for CM 13 and TM 2 gave χ_S/χ_D values of 0·99 and 0·96, respectively, for the Batchelor extension.

5. Conclusions

General

The hypothesis that the small-scale fluctuations of turbulent velocity and scalar fields are statistically independent of the details of the large-scale fluctuations from which they are generated was tested by comparing absolute measurements of velocity and scalar spectra after co-ordinate transformations to length, scalar and time scales formed from the diffusivities (ν/D) and dissipation rates (ϵ/χ) of the velocity and scalar fields.

The local-isotropy similarity-hypothesis prediction of inertial subranges with velocity and scalar spectra proportional to wave-number to the $-\frac{5}{3}$ power was demonstrated experimentally, as well as a viscous-convective subrange in the scalar spectrum proportional to wave-number to the -1 power. Based on these successful predictions from local-isotropy theory and Kolmogoroff-like similarity hypotheses, the curves to which the measured spectra reduce after co-ordinate transformation appear to be universal equilibrium spectra for turbulent velocity and scalar fields. Absolute measurements of transverse spectra would provide valuable further comparison, but none seem to be available.

Velocity field

(1) The velocity spectra measured in the water tunnel, when normalized using the dissipation rate indicated by Batchelor & Townsend's decay law, were in agreement with grid turbulence spectra measured in wind tunnels by Stewart & Townsend. The agreement is taken as an indication that the dissipation rate used was correct, that the hot-film anemometer was a satisfactory device for measuring turbulence in water, and that the spectra of the flow fields in water and air were similar.

(2) The agreement of the transformed spectra for grid turbulence in air and water with turbulent spectra measured in the ocean supports the conclusion that for the highest range of wave numbers the spectrum function shown in figure 3 is universal. Grant *et al.* (1962) found that the normalized dissipation spectrum for their data was in agreement with normalized dissipation spectra taken in shear flow systems.

(3) The universal one-dimensional Kolmogoroff constant for the inertial subrange indicated by the velocity measurements in the water tunnel was $\alpha_1 = 0{\cdot}44 \pm 0{\cdot}02$, corresponding to a three-dimensional constant $\alpha_3 = 1{\cdot}34 \pm 0{\cdot}06$.

Scalar field

(1) A technique was developed capable of measuring R.M.S. conductivity fluctuations as low as 0·003 % (signal-to-noise ratio of one), corresponding to $c'/C = 0{\cdot}003$ % or $t' = 0{\cdot}001$ °C. The maximum spatial resolution was obtained with a 10 μ electrode probe whose response was down 3 dB at a wave-number of about 150 cm^{-1}, equivalent to a wavelength of 0·4 mm (CM 13).

(2) The decay of scalar variance behind the grid was found to obey the following equation

$$\overline{\theta^2}/\theta_0^2 = 3{\cdot}10(x/M)^{-\frac{3}{2}},$$

where θ is the fluctuating component of the scalar field, θ_0 is the change in the mean value of Θ for the fluid as it passes through the grid, x is the distance from the grid, and M is the mesh length. The relation was tested for concentration and temperature mixing, x/M values between 20 and 80, mean velocities from 60 to 210 cm/sec, c_0/C values from $\frac{1}{10}$ to 1 %, and for M values of 1·59 and 2·62 cm.

(3) The transformed scalar spectra indicated a universal scalar inertial Kolmogoroff constant $\beta_1 = 0{\cdot}35$ or $\beta_3 = 0{\cdot}58$. The transformed concentration-mixing spectra exhibited viscous-convective subranges with universal scalar viscous-convective Kolmogoroff constant

$$\beta_2 = (\phi_\theta(k_1)\, k_s^3 \nu/\chi)\,(k_1/k_s) = 2$$

in agreement with Batchelor's recommended value of the effective average least principal rate of strain $\gamma = -1/2(\epsilon/\nu)^{\frac{1}{2}}$.

(4) By comparing the dissipation rates (χ) indicated by the measured spectra with those calculated from the scalar decay law, it was concluded that the spectral measurements at high wave-number were affected by inadequate spatial resolution of the conductivity probes. The actual spectrum must be a smooth extrapolation of the measured data obeying the restriction $\chi_S = \chi_D$; Batchelor's prediction of the universal equilibrium scalar spectrum is consistent with the experimental data for at least the range of wave-numbers shown in figure 9.

The authors gratefully acknowledge the financial assistance of the National Science Foundation under grants G-5506 and G-12141.

REFERENCES

BATCHELOR, G. K. 1953 *The Theory of Homogeneous Turbulence.* Cambridge University Press.

BATCHELOR, G. K. 1959 *J. Fluid Mech.* **5**, 113.

BATCHELOR, G. K. & TOWNSEND, A. A. 1948 *Proc. Roy. Soc.* A, **193**, 539.

CORRSIN, S. 1951 *J. Appl. Phys.* **22**, 469.

CORRSIN, S. 1961 *J. Fluid Mech.* **11**, 407.

GIBSON, C. H. 1962 Ph.D. Dissertation, Stanford University.

GIBSON, C. H. & SCHWARZ, W. H. 1963 *J. Fluid Mech.* **16**, 357.

GRANT, H. L., STEWART, R. W. & MOILLIET, A. 1960 *Pac. Nav. Lab. Rep.* 60–8.

GRANT, H. L., STEWART, R. W. & MOILLIET, A. 1962 *J. Fluid Mech.* **12**, 241.

HINZE, J. O. 1959 *Turbulence.* New York and London: McGraw-Hill Book Co.

KOLMOGOROFF, A. N. 1941 *C.R. Acad. Sci., U.R.S.S.* **30**, 301.

KRAICHNAN, R. H. 1959 *J. Fluid Mech.* **5**, 497.

LING, S. C. 1955 Ph.D. Dissertation, University of Iowa.

OBUKHOFF, A. M. 1949 *Izv. Akad. Nauk. SSSR Geogr. i Geofiz.* **13**, 58.

STEWART, R. W. & TOWNSEND, A. A. 1951 *Phil. Trans.* A, **243**, 359.

UBEROI, M. S. & KOVASZNAY, L. S. G. 1953 *Quart. Appl. Math.* **10**, 375.

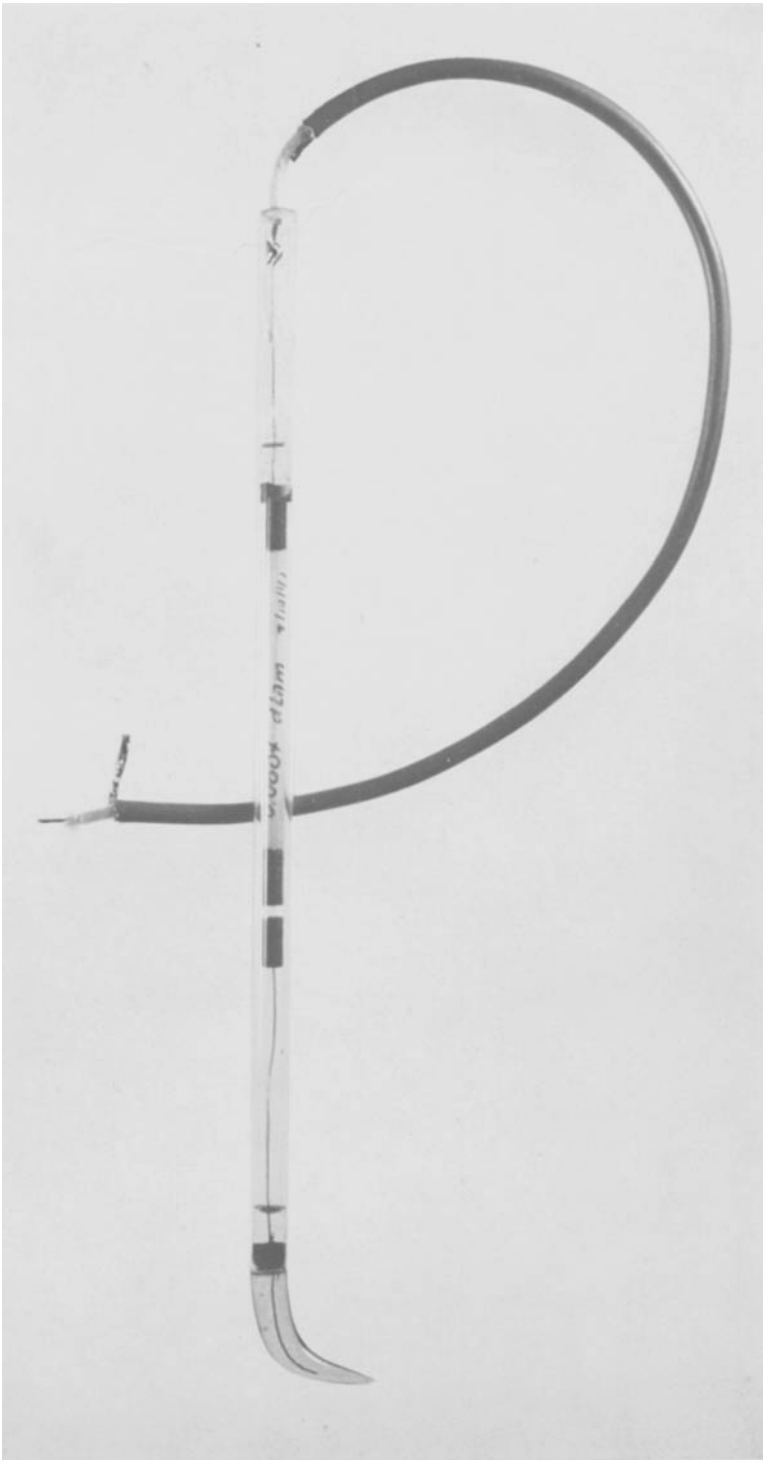

FIGURE 2 (*a*). 10 μ single-electrode conductivity probe; (*a*) probe; (*b*) probe tip.

FIGURE 2(*b*). For legend see plate 1.